Microseismic network sensitivity in case of no seismic activity

Eva Káldy (eva.kaldy@natur.cuni.cz)

Institute of Hydrogeology, Engineering Geology and Applied Geophysics; Faculty of Science Charles University Faculty of Science Albertov 6, 128 43 Praha 2 www.natur.cuni.cz/en https://orcid.org/0000-0001-8395-2071

Tomáš Fischer

Institute of Hydrogeology, Engineering Geology and Applied Geophysics; Faculty of Science Charles University Faculty of Science Albertov 6, 128 43 Praha 2 www.natur.cuni.cz/en https://orcid.org/0000-0002-5169-2567

Research Article

Keywords: local seismic activity, sensitivity of seismic network, seismic monitoring, induced seismicity, microseismicity, West Bohemia / Vogtland

Posted Date: October 14th, 2021

DOI: https://doi.org/10.21203/rs.3.rs-968364/v1

Microseismic network sensitivity in case of no seismic activity

Eva Káldy[1*] and Tomáš Fischer[1]

[1*]Institute of Hydrogeology, Engineering Geology and Applied Geophysic, Faculty of Science, Charles University, Albertov 6, Prague, 120 00, Czech Republic.

*Corresponding author(s). E-mail(s): eva.kaldy@natur.cuni.cz;

Abstract

Underground human activities, such as mining, shale gas and oil exploitation, waste-water disposal or geo-thermal plants, can cause earthquakes. These industry projects need to be monitored by local seismic networks in order to contain the risk. An ideal seismic network should have a triangulated grid, with spacing equal to the depth of the industrial activity with no associated industry noise. In many cases, stations are placed near noisy roads, factories or in a private garden, none of which are located at optimal nodes and which thus introduce great variations in the nose level. In this article, we present a work-flow to determine the sensitivity of any local network, even if there is no local event recorded. In other words: how small are the earthquakes that such seismic networks detect? This knowledge can be used as an argument for claiming an area to be seismically silent-inactive down to a certain magnitude or for evaluating the effect of an additional seismic station. A brief theory and work-flow description is followed by two real-case demonstrations from Czech Republic, Europe: first, a proof-test on a well-studied seismically active area of West Bohemia / Vogtland and second, an application to an uprising geothermal project in Litoměřice, where no seismic activity was detected in years of monitoring.

Keywords: local seismic activity, sensitivity of seismic network, seismic monitoring, induced seismicity, microseismicity, West Bohemia / Vogtland

1 Introduction

The need for CO_2 free sources of energy has seen an increase inf solar, wind, hydrothermal and nuclear power plants, many of which require-local monitoring of micro-earthquakes. Nuclear power plants are monitored to ensure seismic stability of the bedrock (Dojcinovski et al, 2001), and hydrothermal potential induced seismicity (in 2006 water injection to a depth of 5 km induced a M_L 3.4 in Basel, Switzerland; Häring et al, 2008). Both types of power plants are likely to be built in a region with no known seismic activity. This paper presents a proof-tested work-flow to calculate the sensitivity of a local seismic network in a seismically inactive region. Knowing the sensitivity of a local seismic network in 3D is also beneficial for monitoring other underground operations, such as hydraulic fracturing (which caused M_L 2.3 and 1.5 in Blackpool, United Kingdom; Clarke et al, 2014), waste-water injection (in 2011 this was related to M_W 5.7 in Oklahoma, USA; Janská and Eisner, 2012) or gas extraction (Baranova et al, 1999). High sensitivity of a network is one of the arguments for claiming that the area is secured/seismically silent-inactive and therefore suitable for building industry projects such as power plants, nuclear waste disposal or, in our case, a geothermal project.

The ability of a seismic network to detect local micro-earthquakes is a function of the number of

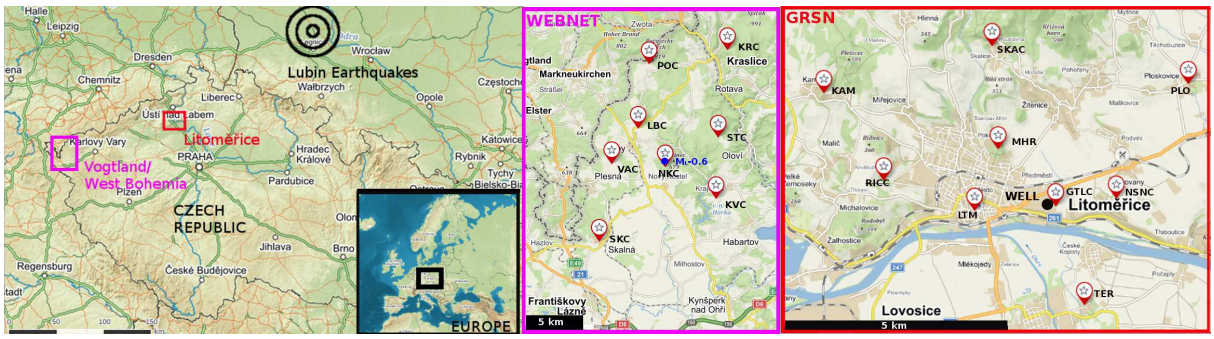

Fig. 1 **Left:** Region overview with highlight of West Bohemia region in magenta and Litoměřice in red. **Center:** WEBNET: map of subset of seismic network in Vogtland/West Bohemia - 8 stations used for event detection by PePin detector. Location of a weak M_L - 0.6 event as blue circle. **Right:** GRSN: Map of permanent stations of the seismic network in Litoměřice (station RICC unreliable and so omitted in this study). Location of future hydrothermal well by black circle. (map background by mapy.cz)

stations, their location, seismic noise, local geology and the detection method. The sensitivity of a seismic network is a spatial monitoring performance in terms of the smallest reliably detectable magnitude, ideally presented in the form of a 3D map, but, in the case of insufficient information, also by a single value representing the magnitude of completeness M_C of the whole network. From the catalog completeness M_C we can determine the magnitude at which the cumulative frequency magnitude distribution deviates from Gutenberg-Richter law (Wiemer and Wyss, 2000; Leptokaropoulos and Gkarlaouni, 2016). Various methods have been proposed to determine network sensitivity. A theoretical sensitivity using the moment magnitude, that also depends on the velocity and density model, is presented in Hallo (2012). When a seismic network is already operating, the sensitivity can be tested using synthetic seismic events overlying the real seismograms (López-Comino et al, 2017), or by comparing the P_n amplitude-distance curve to the signal-to-noise ratio (Sereno Jr. and Bratt, 1989). In the case of a highly active and long-term monitored region, the sensitivity is calculated from seismic catalogs (Mignan et al, 2011; Fischer and Bachura, 2014) or can be derived continuously (Kværna et al, 2002).

In this paper, we propose a new method to evaluate the 3D sensitivity of a local network that has no recorded local seismic activity. The sensitivity is based on a theoretical S-wave signal that exceeds the noise level at numerous stations. To calibrate this approach, we adopt the local magnitude M_L calculation used in West Bohemia / Vogtland region (Horálek et al, 2000, revisited by Čermáková and Horálek, 2015), which is a function of the maximum S-wave velocity and the hypocentral distance. This is converted into a function of station's noise level and real-scenario peak-to-noise ratio. Such 3D sensitivity is derived for two local seismic networks in the Czech Republic: WEBNET in West Bohemia for proof-testing the concept using existing local seismic activity and the GRSN in Litoměřice for its application

1.1 Local seismic networks

The aim is to derive the sensitivity of a local GRSN network that monitors the RINGEN geothermal project (Šafanda et al, 2020) that is being built near Litoměřice, a town in central Bohemia, Czech Republic (Fig. 1). An Enhanced Geothermal Systems (EGS) was originally planned at 5 km depth and a pilot 2.1 km deep geothermal borehole was drilled in 2007. At present, the RINGEN seismic network (GRSN) consists of nine surface stations (spaced 1.5 - 4.5 km apart, one of which is unreliable and was omitted in this study) and two down-hole receivers (these were not present at the beginning of this study, so they were omitted). The first two surface stations were installed in 2013, the surface network was completed in 2019 and the downhole receivers started recording in July 2020. Although an efficient automatic detection algorithm PePin, based on the method of Fischer (2003) was implemented in 2019, no local seismicity has been detected in the Litoměřice region so far, nor by the Czech Regional Seismological

Network (Charles University in Prague (Czech) et al, 1973). The most recent algorithm setting requires the detection of at least one P-wave and four S-wave arrivals; the fact that local seismicity data is missing prevents us from determining the network sensitivity using standard methods mentioned above, which motivated us to derive an approach based on known information.

The proof-test region for our method of seismic network sensitivity is a seismologically active area of West Bohemia (Fig. 1 center) in Czech Republic, which borders Vogtland in Saxony, Germany (Neunhöfer and Hemmann, 2005). Most of the seismic swarms occur in the Nový Kostel (station NKC) region at 6 - 10 km depth with local magnitudes up to M_L 3.8 in 2008 (Čermáková and Horálek, 2015). All the 23 permanent stations of the WEBNET seismic network (Institute of Geophysics, Academy of Sciences of the Czech Republic, 1991) stream data in real time. Two methodologies are used nowadays for data processing: automatic detection and location by the detector (Fischer, 2003) and neural-network (Doubravová from Institute of Geophysics, Academy of Sciences of the Czech Republic, personal communication). Neural-network detections are manually picked and located; events $M_L > 0$ are presented online. The automatic detection algorithm PePin analyses the waveforms of 8 stations (spaced 4 - 8 km apart) surrounding the most active area of Nový Kostel and the results are published online in near real time. It is this eight-station subset that we use in our study.

2 Methodology

By the sensitivity of a seismic network we understand a 3D map of the minimum detectable magnitude, when considering reasonable limits of an applied earthquake detection method. The calculated seismic network sensitivity is focused on networks such as the Litoměřice area where stations are separated by only a few kilometers, without any known seismic activity and with potential seismic activity in the first few kilometers underground. This setting allows us to draw the following assumptions:

First, for a seismically inactive region, the detection algorithm utilizing a signal amplitude that exceeds the background noise level is to be used. The reason is that the more sensitive methods, such as cross-correlation (Janská and Eisner, 2012) or neural network (Perol et al, 2018; Doubravová and Horálek, 2019) require knowledge of the waveform(s) of local seismic events, which is missing in the area of interest.

Second, in the far field, S-wave amplitudes are greater than P-wave amplitudes depending on the reciprocal of the third power of wave velocity (e.g. Shearer (2009) and an example in Fig. 2), especially on horizontal components, and there are very weak, if any, surface waves. This means that it is the S-wave signal (above noise level) that triggers the detection algorithm, especially for the weak events. Therefore, if the magnitude is determined using the S-wave peak amplitude, the minimal detectable magnitude is a function of the noise level of the horizontal components of the triggering station. Note that instead of using the Signal to Noise Ratio (SNR), where the signal value is an average over a short time window, as used for the sta/lta (Trnkoczy, 2012), we use (S-wave) Peak to Noise Ratio (PNR) because it is directly connected to the magnitude calculation (section 2.3).

Third, usually a seismic event must trigger at minimum three stations in order to be locatable, but due to the S-wave radiation pattern, these triggering stations are not necessarily only the closest ones. An example of a local event M_L -0.6 is shown in Fig. 2, where the waveforms are arranged according to the distance to the event, but the second closest station LBC shows a significantly smaller Peak to Noise Ratio (PNR). This LBC station, together with station KVC, lies on the fault nodal plane. To account for the focal mechanism effect on amplitudes, we decided to set the algorithm to use one additional station to the number of stations required to trigger S-wave.

2.1 Noise level

Each station is characterized by its noise level, which is a function of human activity, weather, geology and time. Assigning a single value characterizing such complex behavior is tricky and different statistical approaches can be taken. In our case, the noise value is defined as the root-mean-square (RMS) of filtered waveforms; due to the application of the L_2 norm, the noise level value is sensitive to noise bursts or artificial noise peaks, which are likely to cause false triggers,

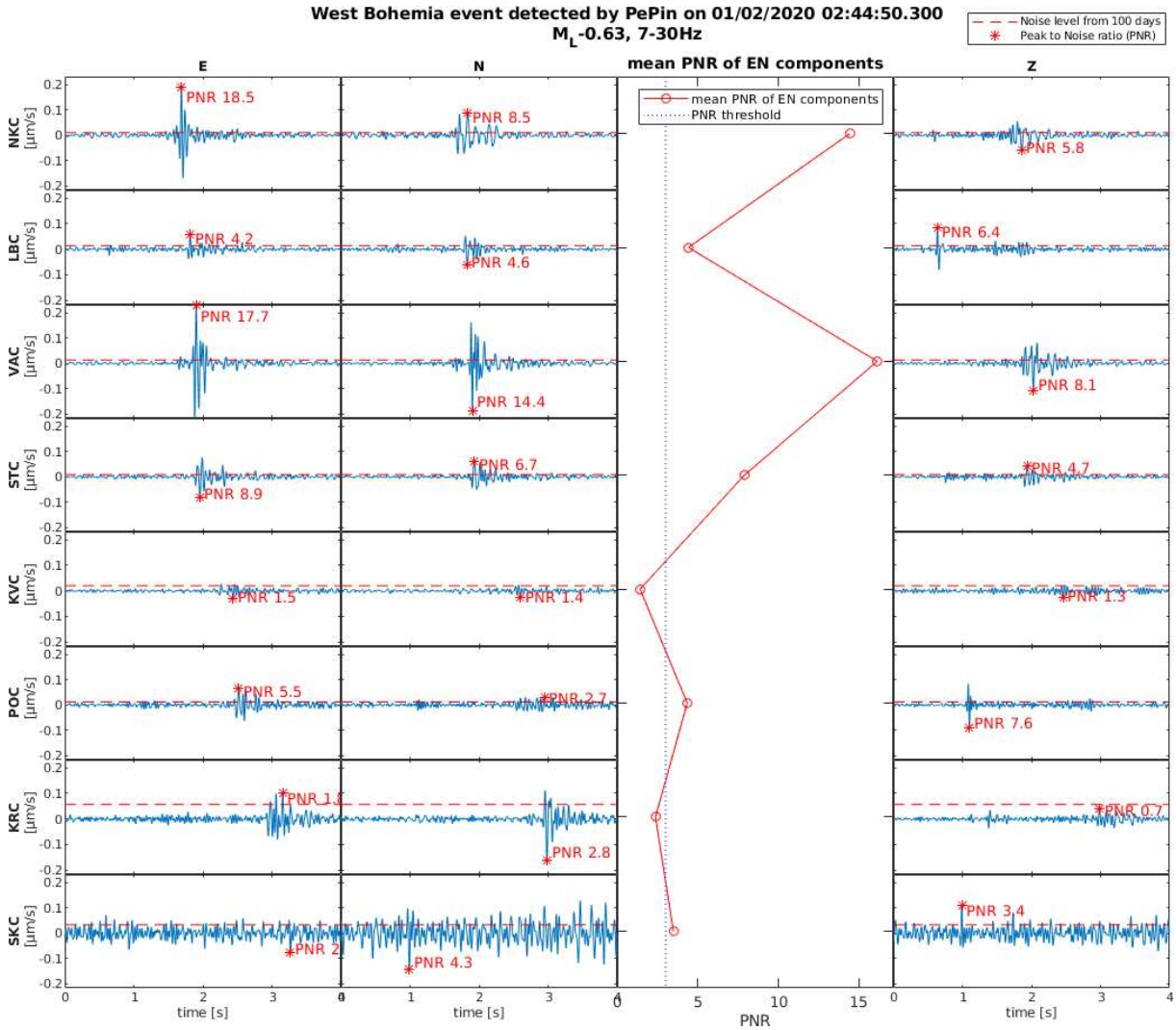

Fig. 2 A weak local seismic event near Nový Kostel, West Bohemia automatically detected and located by PePin with two P-waves and six S-waves on 2^{nd} January 2020 02:44:50 UTC. Automatically assigned M_L -0.6, depth 8 km, latitude 50.2522, longitude 12.4444. Blue waveforms are filtered 7-30 Hz and have similar scales in μm/s. Red dashed line shows noise level from 100 days, which in this case is high above real noise on stations KVC and KRC. Red star highlights the highest peak in display (in SKC it does not represent event waveform) labeled with corresponding PNR. A subplot with mean PNR of horizontal (EN) components shows that the value of PNR is not a smooth function of distance from the source (stations are sorted by distance), but the second closest station has the fourth greatest PNR. Six PNR values are above the triggering threshold (PNR = 3), although the triggering stations differ from PePin triggering one.

making noisy stations less useful for detection. The RMS method therefore fails in stations with extreme values of spikes and these need to be handled individually, for example by advanced filtering.

We searched for an optimal band-pass filter similar for both GRSN and WEBNET that would suppress major noise and enhance the high frequency signal of weak local events. Spectrograms of GRSN stations showed coherent 35 Hz noise at PLO station and therefore the upper cutoff frequency was set to 30 Hz. Several lower cutoff frequencies were tested on weak events from WEBNET, and the filter 7-30 Hz proved to give the highest peak-to-noise ratio (PNR) when tested on weak events (see an example of the effect of three different band pass filters on East component of event M_L -1.1 from 2018 in Fig. 1 in the supplement). Therefore, this study uses

Table 1 Station's noise level is the RMS of horizontal components filtered 7-30 Hz from the first 100 days of year 2020. Red background indicates the noisiest stations, green the quietest ones.

GRSN – noise level [μm/s]									
	NSNC	SKAC	KAM	MHR	TER	PLO	GTCLT	LMP	average
	0.04	0.09	0.12	0.15	0.24	0.34	0.52	0.56	0.26
std	0.03	0.06	0.09	0.08	0.16	0.23	0.37	0.3	0.17
WEBNET – noise level [μm/s]									
	STC	NKC	POC	LBC	VAC	KVC	SKC	KRC	average
	0.009	0.01	0.012	0.013	0.013	0.02	0.033	0.057	0.021
std	0.006	0.006	0.008	0.008	0.008	0.011	0.006	0.015	0.009

waveforms filtered by 7-30 Hz, unless mentioned otherwise.

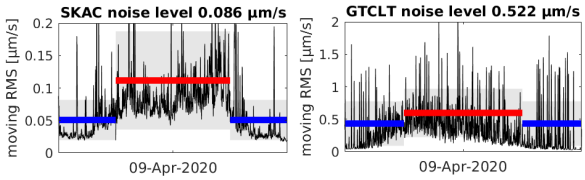

Fig. 3 GRSN: low noise station SKAC on left, noisy station GTCLT on right. RMS noise level during day (red) and night (blue) overlying smooth record (moving RMS in 100s window, black) from a working day (Thursday 9^th April 2020). Standard deviation of 100 day/night values highlighted by shadowed areas. Note that the noise y-scale varies by 10 times.

Since the S-wave is essential for our approach, it is practical to take in account only the horizontal components, which carry most of the S-wave signal. The noise level in Table 1 was calculated from the horizontal components of the first 100 days of the year 2020 because there was only minor seismic activity in West Bohemia. The average noise level of seismic networks varies by 10 times: 0.021 μm/s in West Bohemia and 0.26 μm/s in Litoměřice. Such a difference is also inside a network, as presented in Fig. 3 on SKAC and GTCLT station from GRSN. Day/night variation of noise is more pronounced in GRSN. These differences are likely due to differences in geology and because the noisier GRSN stations are situated at busy/industrial spots. To show the relevance of the noise level, the noise level is displayed as a red dashed line over real event waveforms of WEBNET stations in Fig. 2.

2.2 Detection algorithm

The automatic detection algorithm (PePin) operating both in West Bohemia and Litoměřice requires the recognition (trigger) of at least one P-wave and four S-wave arrivals. It is the smallest recognized S-wave amplitude that defines the triggering peak-to-noise ratio (PNR) of an event. To find a representative minimal triggering PNR, we analyzed the PNR of detected WEBNET events from the first 100 days of the year 2020, when only weak background seismic activity occurred. This allowed us a visual examination of the waveforms and to understand the outcome of detection.

A total of 242 events were automatically detected and located 10x10 km around NKC. If these events were not also detected by the neural-network, their waveforms were visually checked. As presented in Fig. 2 in the supplement, we identified 11% of false detections (27 events, 12 of which are distant events with incorrect locations). These false detections had no effect on the overall magnitude of catalog completeness (M_C -0.4), when derived as the maximum of magnitude distribution (deviation from Gutenberg-Richter law in Wiemer and Wyss, 2000). Note, that the neural-network detected an additional 45 events above M_C in this region, but this might be because the PePin locations of corresponding events were outside the selected region.

The triggering PNR of each event was derived, using the noise level of the corresponding station. As illustrated in the supporting plots in the supplement Fig. 3 (top 2 charts), the triggering peak-to-noise ratio of the 242 detections mentioned begins at PNR 2, but only 17 of 215 real events occurred with PNR<3, which makes the threshold PNR 3 a reasonable input for the sensitivity calculation. A further positive indication is that the PNR 3 removes 10 of 17 false detections. It was also tested to determine whether the number of triggering stations correlates with the event magnitude and depth. Unfortunately, no such relation was observed (see Fig. 3 bottom chart in supplement).

2.3 Local magnitude

The amplitude of a seismic signal recorded at a station is a function of the event magnitude, the distance between the earthquake and the station, the earthquake mechanism and a local amplification. We adopt the following formula for magnitude calculation that is used at the WEBNET in West Bohemia / Voglant (Horálek et al,

Table 2 GRSN station corrections with corresponding standard deviation derived from 48 seismic events $M_L > 2.5$ from Lubin region, Poland. Stations sorted by the noise level.

Station	NSNC	SKAC	KAM	MHR	TER	PLO	GTCLT	LMP
C_i	0.398	-0.346	0.017	-0.508	0.083	0.093	0.067	0.196
δ_i	0.15	0.13	0.14	0.13	0.15	0.14	0.47	0.13

2000, revisited by Čermáková and Horálek, 2015):

$$M_{Li} = \log(A_{S_{max}}) - \log(2\pi) + \\ + 2.1 * \log(R_i) + C_i - 1.2$$

where M_{Li} is a local magnitude derived at the i^{th} station, $A_{S_{max}}$ is an absolute value of the maximum total amplitude of the S-wave ground velocity measured in μm/s, R_i is the hypocentral distance of the i^{th} station in kilometers, and C_i is the station correction. Each event is represented by an average magnitude M_L. The maximum errors are $\pm 0.2 M_L$, when only a subset of 4 to 5 stations is used (Čermáková and Horálek, 2015). It is not linked to any regional magnitude.

Transferability of this local magnitude calculation to the Litoměřice region was tested on regional events from Lubin (Poland, Fig. 1 left). Only 48 Lubin events with $M_L > 2.5$ had a signal above the noise level, both in West Bohemia and Litoměřice in the first half of the year 2020. To enhance the peak-to-noise ratio of such regional events, the waveforms were filtered 1-10 Hz. Magnitude was calculated from the peak amplitudes of the horizontal components, without any station correction. Each station shows a bulk shift between reported M and calculated M_L. Network corrections were derived as the mean difference of the station M_L bulk shifts. This is similar for both networks: M_L 0.65 for GRSN and M_L 0.54 for WEBNET. Station corrections C_i were derived correspondingly and WEBNET station corrections are in accordance with the station corrections given in Čermáková and Horálek (2015) (Fig. 4 in the supplement). The similarity of network correction and correspondence of station corrections for WEBNET shows that the formula for local magnitude from West Bohemia is transferable to the Litoměřice region as is. Resulting station corrections of GRSN stations are presented in Table 2.

2.4 Simplified workflow

Knowing parameters such as a station's noise level and location, minimal PNR for detection and the required number of triggering stations (T), the area of potential earthquakes is represented by a 3D grid of the station's locations. For each grid point (x, y, z) the minimum detectable magnitude for station i is computed as

$$M_{Li}(x,y,z) = \log(N_i * PNR) - \log(2\pi) + \\ + 2.1 * \log(R_i) + C_i - 1.2 \quad (1)$$

where N_i is the noise level in μm/s and PNR represents the minimum triggering PNR of the S-wave (3 in our case). The minimal detectable magnitude at a point (x, y, z) is the $(T+1)^{th}$ smallest value of M_{Li} (5^{th} in our case).

3 Network sensitivity results

A highly sensitive seismic network can detect earthquakes of smaller magnitudes than a less sensitive one. Quantification of network sensitivity is done using the minimal magnitude that a network can detect. The network sensitivity calculation presented here is a function of the location of the seismic station, the station's representative noise level, detection algorithm parameters such as PNR and the number of triggering stations and the area of interest defined by its coordinates. Since all the factors are known or calculated for both the West Bohemia and Litoměřice region, the corresponding sensitivities are presented below.

3.1 West Bohemia region

The noise levels for the simulation of WEBNET sensitivity were derived using seismograms from the first 100 days of the year 2020, the station corrections were adopted from Čermáková and Horálek (2015), the condition of PNR>3 was outlined in section 2.2 Detection algorithm; the

requirement of 5 triggering stations resembles the 4 triggering stations of the applied automatic detection algorithm.

The results of the application of the equation 1 to WEBNET are displayed as a 3D view in Fig. 4. To relate the sensitivity to the known seismicity, the sensitivity cross sections are overlaid by seismic activity in years 2016-2021 in Fig. 5. It shows that the known seismicity lies in the region of the network with sensitivity starting at M_L -1.3 near Nový kostel (NKC) at depth 6 km and going down to M_L -0.8 for the south flank activity (between SKC and KVC) at depth of 10 km.

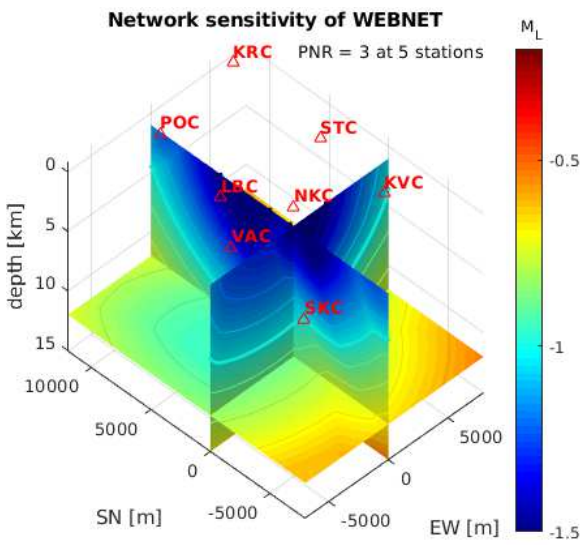

Fig. 4 WEBNET: Network sensitivity as the **minimal detectable magnitude** M_L. Isolines are spaced by M_L 0.1, bolder ones are multiples of M_L 0.5. Seismic stations are shown by red triangles with the station names.

Since the simulation of network sensitivity in Fig. 4 and 5 follows the setting of the automatic detection algorithm (triggering PNR 3 at a minimum 5 stations), the sensitivity is expected to correspond to the minimal detectable magnitude of the detection algorithm. To check this expectation, the calculated sensitivity is compared to the network sensitivity derived from the events automatically detected by PePin in 2014-2018. To achieve a meaningful comparison, both simulations and catalog data were confined to the area of greatest activity, i.e. a 2x4 km rectangle NE of Nový Kostel (NKC) at a depth of between 6 and 11 km, see Fig. 6. The simulation is represented by an average sensitivity at corresponding depth slices (yellow triangles with the corresponding M_L in yellow). The result of automatic detection is represented both by individual event hypocenters (blue circles) and by the magnitude of catalog completeness M_C at each depth slice +/-0.5 km (red stars). Interestingly, the simulated minimal detectable magnitudes envelop the very weakest catalog events. Another alignment between the simulated and real sensitivity is demonstrated for an active area at the South flank of the network and the setting and results are shown in the supplement in Fig. 5.

To conclude, the proof-test of the seismic network sensitivity calculation provides a great fit for the minimal detectable magnitude when the setting is in line with the detection algorithm parameters.

It would be more convenient to simulate the network sensitivity in terms of the magnitude of catalog completeness M_C instead of minimal detectable magnitude. Unfortunately, the number of triggering stations does not correlate with the magnitudes of detected events (Fig. 3 bottom chart in supplement), therefore a more engineered approach was taken. Using a conservative criterion of two additional triggering stations makes the depth variation of the simulated sensitivity fairly consistent with the catalog-derived M_C (green triangles with labels compared to red stars, Fig. 11 left). The WEBNET sensitivity simulation with 7 triggering stations shows simulated M_C variation M_L -0.7 to M_L -0.4 between 6 and 11 km in the high activity zone. Depth cross sections of simulated M_C are displayed in Fig. 7, which shows two highly sensitive regions: first triangle in the SouthEast of the network, and second an ellipsoid in the North-West area of the network.

3.2 Litoměřice region

The noise level and station corrections for the simulation of GRSN network sensitivity were derived using seismograms of the first 100 days of the year 2020. The PNR>3 assumption is taken from the WEBNET, the requirement of 5 triggering stations resembles the 4 triggering stations of the applied automatic detection algorithm.

The simulations show a sensitivity maximum surrounding the well as expected, with a prolongation in the NW-SE direction, see 3D view in

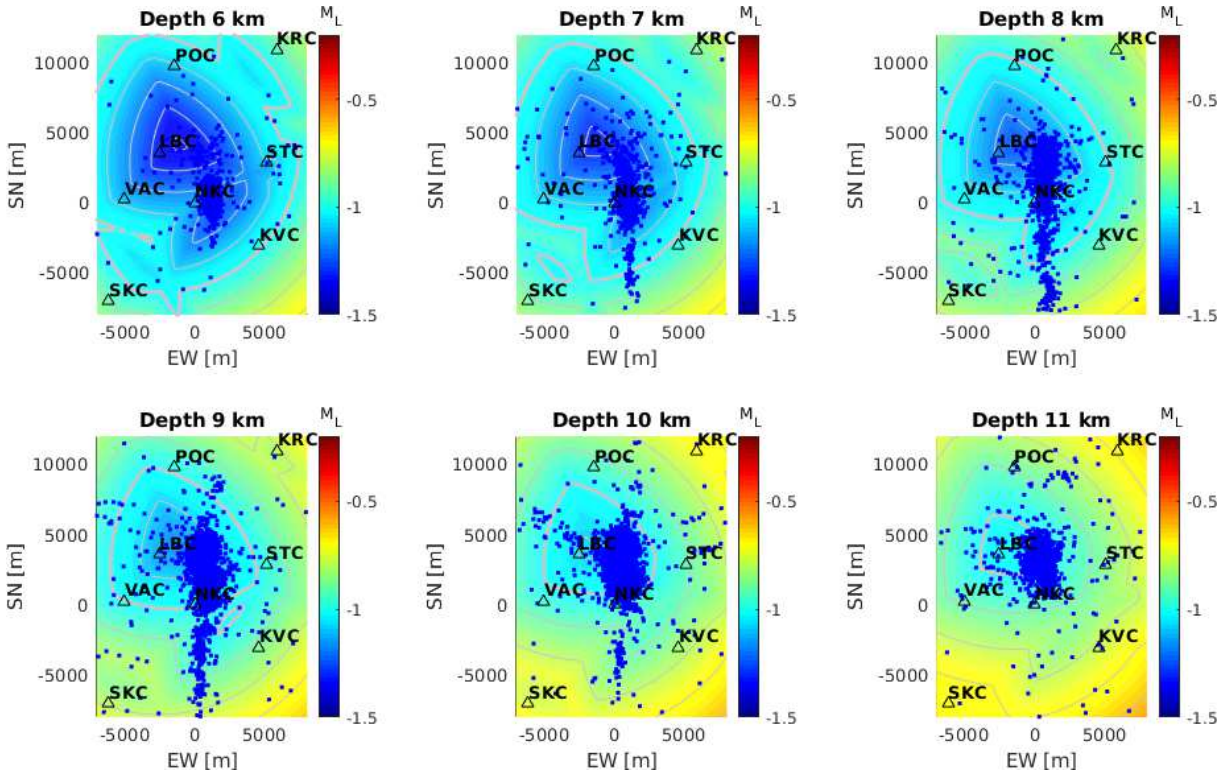

Fig. 5 WEBNET: Network sensitivity as depth slices of the **minimal detectable magnitude** M_L. Grey isolines are spaced by M_L 0.1, bolder ones are multiples of M_L 0.5. Subplot titles note the slice's depth below mean sea level. The sensitivity map is overlain by seismic activity in 2016-2021 in blue points and by seismic stations in black triangles with stations'names.

Fig. 8 and the depth cross sections of between 2 and 5 km in Fig. 9. This means that GRSN starts detecting events from M_L -0.8 and M_L -0.4 at depths of 2-5 km near the well The network sensitivity in terms of the magnitude of completeness was simulated with 7 triggering stations out of the 8 in total. Horizontal slices in Fig. 10 show two conjoined maxima, with the stronger near the LTM station. The magnitude drop in sensitivity between these maxima is M_L -0.3 and it is reduced with depth to nearly zero. Near the well, the maximum detectability completeness varies in depth from M_L -0.6 to M_L 0.1.

If a network operator wants to judge the effectiveness of each station independently, it would be reasonable to look at the minimal detectable magnitude of individual stations. At GRSN it shows that the stations' sensitivity varies greatly (by M_L 1.3 at depth 2 km, Fig. 6 in supplement) which means that the more sensitive half of the stations covers all the area in terms of detection, and the other half is used for detection only in their (limited) surroundings.

4 Discussion/Conclusions

Local scale seismic monitoring uses a grid of stations separated by a few kilometers, but not all of them might actually be enhancing the ability of the seismic network to detect events. The reasons for this is that the recorded noise level, together with station's correction, can undermine the station's sensitivity.

In this paper, we have presented the method and workflow to evaluate the network's sensitivity in 3D, even in cases where there is no local activity recorded. The method was proof-tested in the long-term monitored region of West Bohemia / Vogtland and applied to a geothermal project being constructed in Litoměřice, both in the Czech Republic. The 3D network sensitivity is a function of network geometry, detection algorithm setting and the noise level of each seismic

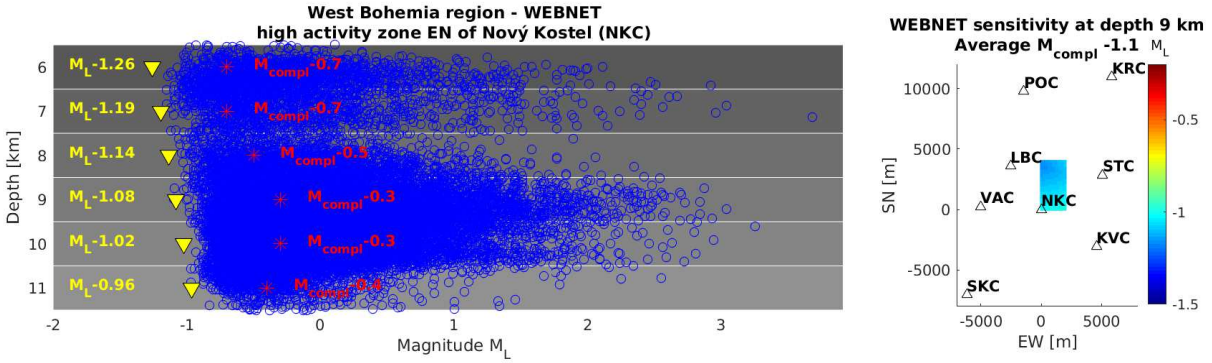

Fig. 6 WEBNET **simulated vs. real sensitivity** in high activity zone. **Left:** Seismic activity as detected by automatic detection algorithm in highly active area NE of Nový Kostel (station NKC). Seismic events displayed as M_L vs depth below mean sea level in blue circles. A magnitude of completeness (red star with red label) is calculated separately for each depth range (gray rectangles in background). Average simulated sensitivity in this region (yellow triangles with yellow labels here, depth layers in supplement in Fig. 5 left) is enveloping the observed seismic activity. **Right:** Map view of the simulated sensitivity at depth 9 km (in color).

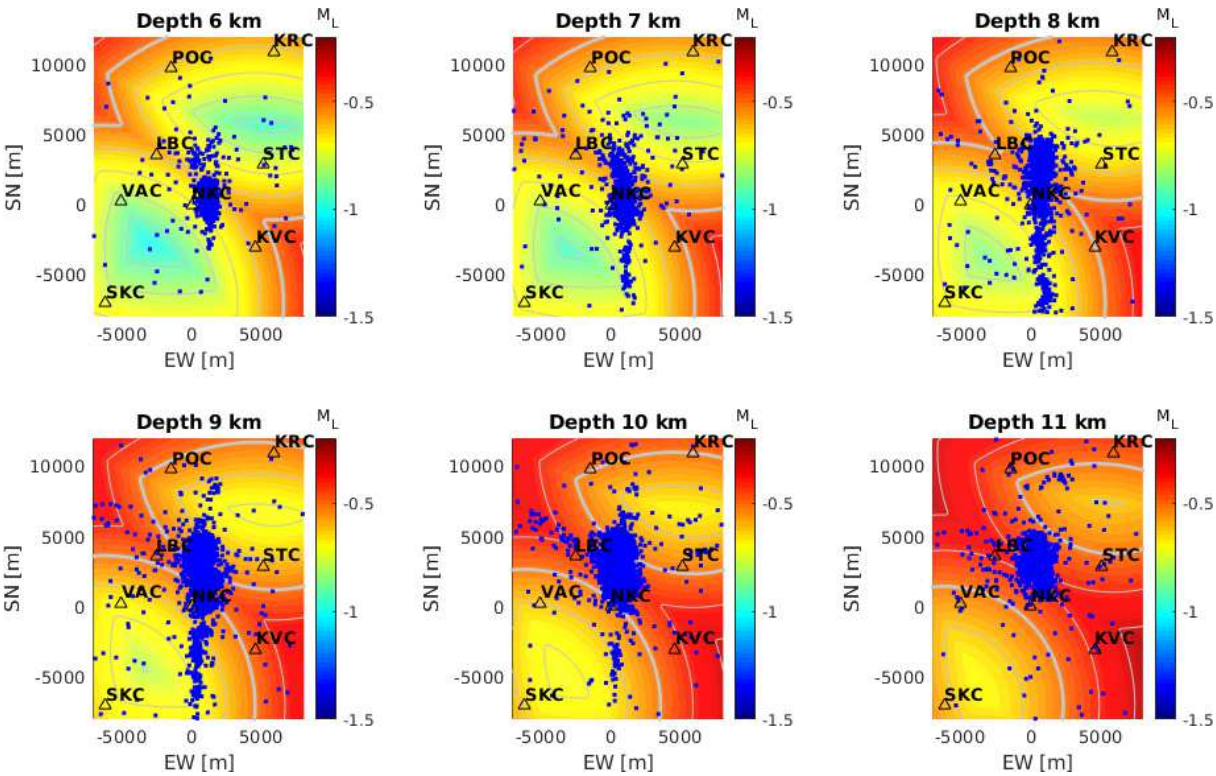

Fig. 7 WEBNET: Network sensitivity as depth slices simulating the **magnitude of completeness** (PNR>3 at 7 of 8 stations). Grey isolines are spaced by M_L 0.1, bolder ones are multiples of M_L 0.5. Subplot titles note the slice's depth below mean sea level. The sensitivity map is overlain by seismic activity in 2016-2021 in blue points.

station. In this study, the sensitivity was simulated as a 3D underground grid, where each point has assigned magnitudes of events causing the signal to equal three times the noise at each station. The resulting network sensitivity at a grid point is the fourth smallest magnitude, in case three stations are required to trigger by the detection algorithm. It is shown that the simulated seismic

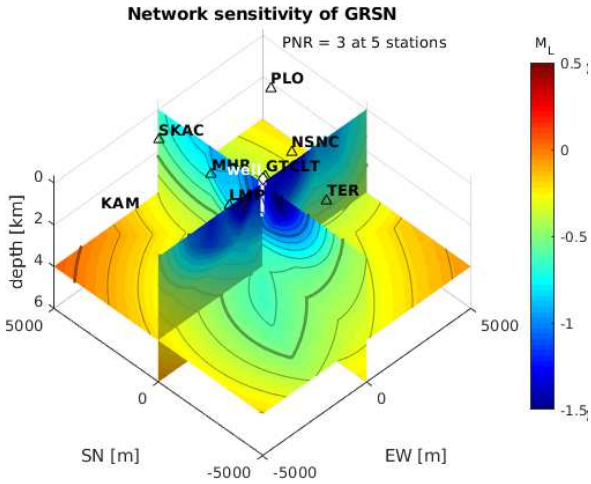

Fig. 8 GRSN: Network sensitivity as the **minimal detectable magnitude** M_L. Grey isolines are spaced by M_L 0.1.

sensitivity corresponds to the weakest detectable earthquakes; the calculation reflects the number of triggering stations required by the detection algorithm. In the case of an additional two triggering stations, the simulated seismic sensitivity correlates with the magnitude of completeness achieved at each grid point. This was shown by overlying the simulated sensitivity over a great amount of detected events, both in an area of a few kilometers and varying in depth (Fig. 11, WEBNET on the left).

Near the planned geothermal well in Litoměřice, the minimal detectable magnitude varies from M_L -1 at depth of 1 km to M_L -0.3 at 6 km depth (Fig. 11, GRSN on the right). Simulations of the magnitude of completeness show that there should not be any seismic activity near the well with a magnitude above zero, that would not be detected at depth 6 km or shallower. No local extremes or steep horizontal decline of sensitivity are present. As such, the area can be considered to be sufficiently monitored and seismically inactive since no local microearthquakes were detected so far.

To find stations that have the least effect on detection, it is possible to look at the minimal detectable magnitude in case only a single station was available. The resulting variation in the sensitivity, for example in an area of interest, is a summation of the stations' noise level and station correction of magnitude. In our study, the variation of sensitivity is M_L 0.6 (from M-1.6 to M-1.0, Fig. 7 in supplement) in WEBNET at a depth of 7 km, showing three weaker stations. The variation in GRSN is greater, M_L 1.3 (from M-2.2 to M-0.9 Fig. 6 in supplement) at a depth of 2 km. It is pointing out that these three stations hardly contribute, if the detection requires 5 stations. This is due to the variation both in noise level (10times, Table 1) and in station correction (difference M_L 0.9, Table 2).

One might ask why the sweet spot of the highest WEBNET sensitivity shifts so significantly and breaks into two when a different number of triggering stations is required (Fig. 7). It is due to the difference in the sensitivity of the individual stations as pointed out above: The sensitive stations dominate the region, and are considered to be triggering even for the farthest events, omitting the closer stations. When only 5 stations are required to trigger, the five most sensitive stations (more blue, Fig. 7 in supplement) cover the whole region, leaving the two least sensitive ones in the SouthEast and NorthWest corner of the network completely unused, even though the event is right below them. When 7 of 8 stations are required to trigger, to simulate the magnitude of completeness, it is these two least sensitive stations that play the main role and so the sensitivity has got two maxima, 5 km NE and SW horizontally from the main activity.

The overall sensitivity of GRSN is weaker than that of WEBNET due to the greater noise from the industry and town of Litoměřice. In the area of interest at a depth of 2 km, the difference is M_L 0.7 (Fig. 11). Another comparison of seismic networks is in terms of sensitivity decline with depth. The decline of GRSN sensitivity (M_L) with depth is steeper than in WEBNET: from 1 to 5 km depth the sensitivity is reduced by M_L 0.3 in WEBNET and by M_L 0.7 in GRSN. The reason for this is that the network sensitivity at a grid point corresponds to the sensitivity of the weakest station that is accounted for in the detection at this grid point. If this weakest station is close, the magnitude M_L decays rapidly with depth (i.e. distance to this station), as is the case in GRSN where the weak stations are a maximum of 4 km from the well. On the other hand, if the weakest stations are further away, the logarithmic magnitude decay with distance is not so rapid and the distance to a station does not change with depth so much. In WEBNET, the span between stations

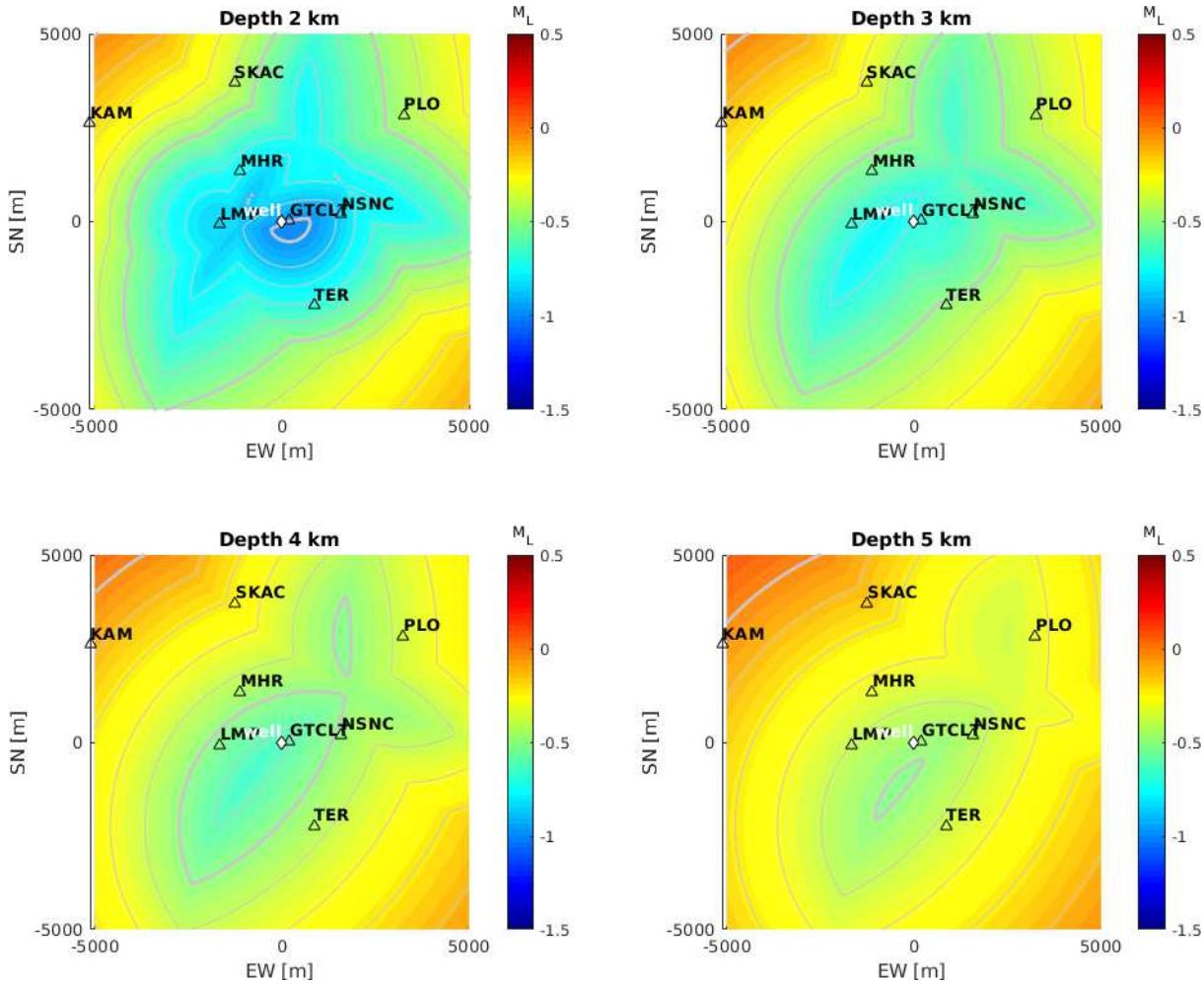

Fig. 9 GRSN: Network sensitivity as depth slices of the **minimal detectable magnitude** M_L, representing the detection of events with PNR>3 at minimum 5 stations. Grey isolines are spaced by M_L 0.1. Subplot titles note the slice's depth below mean sea level. The sensitivity map is overlain by seismic stations in labeled black triangles and the well location as a white diamond.

is greater and the weaker stations are at a 10 - 12 km horizontal distance from the active zone. This is why there is less change of sensitivity with depth in WEBNET as in GRSN.

In conclusion, exploitation of 3D network sensitivity is the visualization of an expected effect when a change in the network geometry or in the setting of a detection algorithm is planned. Another use is in identifying stations of minor/-greatest benefit and an argument for claiming the area well monitored and seismically inactive.

Acknowledgements

I would like to acknowledge Jana Doubravová from Institute of Geophysics, Academy of Sciences of the Czech Republic for insight in the WEBNET seismicity and my colleagues Josef Vlček and Ali Salama for all their support. The research was supported by the RINGEN - research infrastructure upgrade, which is co-funded by the EU Operational Programme Research, Development and Education. The authors declare that they have no conflict of interest. No funding was received for conducting this study.

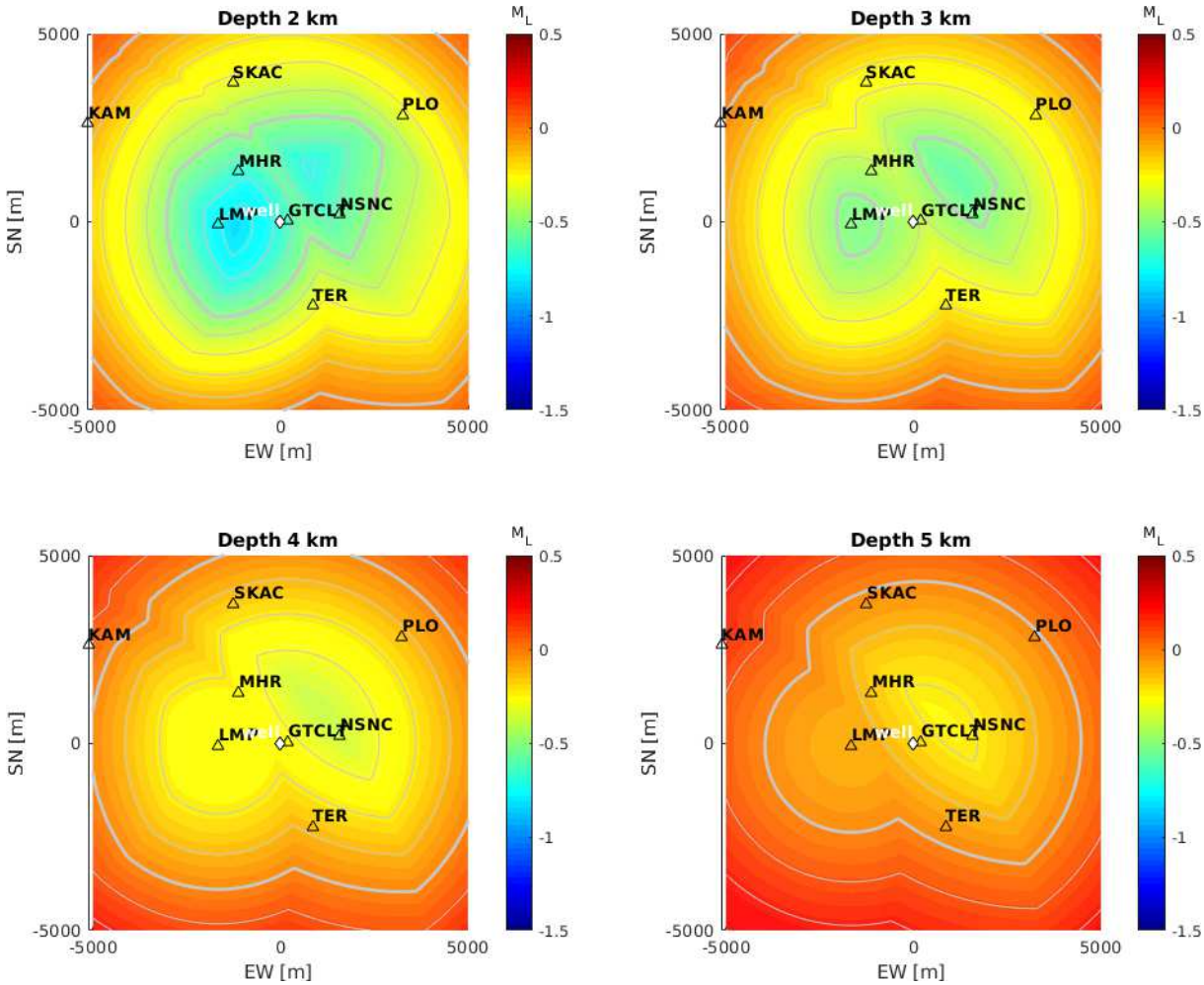

Fig. 10 GRSN: Network sensitivity as depth slices simulating the **magnitude of completeness** (PNR>3 at minimum 7 stations). Grey isolines are spaced by M_L 0.1. Subplot titles note the slice's depth below mean sea level. The sensitivity map is overlaid by seismic stations in labeled black triangles and the well location as a white diamond. Summary of the average minimal and complete magnitude per depth is displayed in Fig. 11 for both GRSN and WEBNET.

References

Baranova V, Mustaqeem A, Bell S (1999) A model for induced seismicity caused by hydrocarbon production in the Western Canada Sedimentary Basin. Canadian Journal of Earth Sciences 36(1):47–64. https://doi.org/10.1139/e98-080

Charles University in Prague (Czech), Institute of Geonics, Institute of Geophysics, Academy of Sciences of the Czech Republic, et al (1973) Czech regional seismic network. https://doi.org/10.7914/SN/CZ, URL https://www.fdsn.org/networks/detail/CZ/

Clarke H, Eisner L, Styles P, et al (2014) Felt seismicity associated with shale gas hydraulic fracturing: The first documented example in europe. Geophysical Research Letters 41(23):8308–8314. https://doi.org/10.1002/2014GL062047

Dojcinovski DM, Mamucevski DJ, Mihailov VP (2001) Seismic Monitoring of Nuclear Power Plants; An Approach to Optimal and More Accurate Seismic Data Processing and Interpretation Procedure, Springer Netherlands, Dordrecht, pp 417–431. https://doi.org/10.1007/978-94-010-0696-5_29

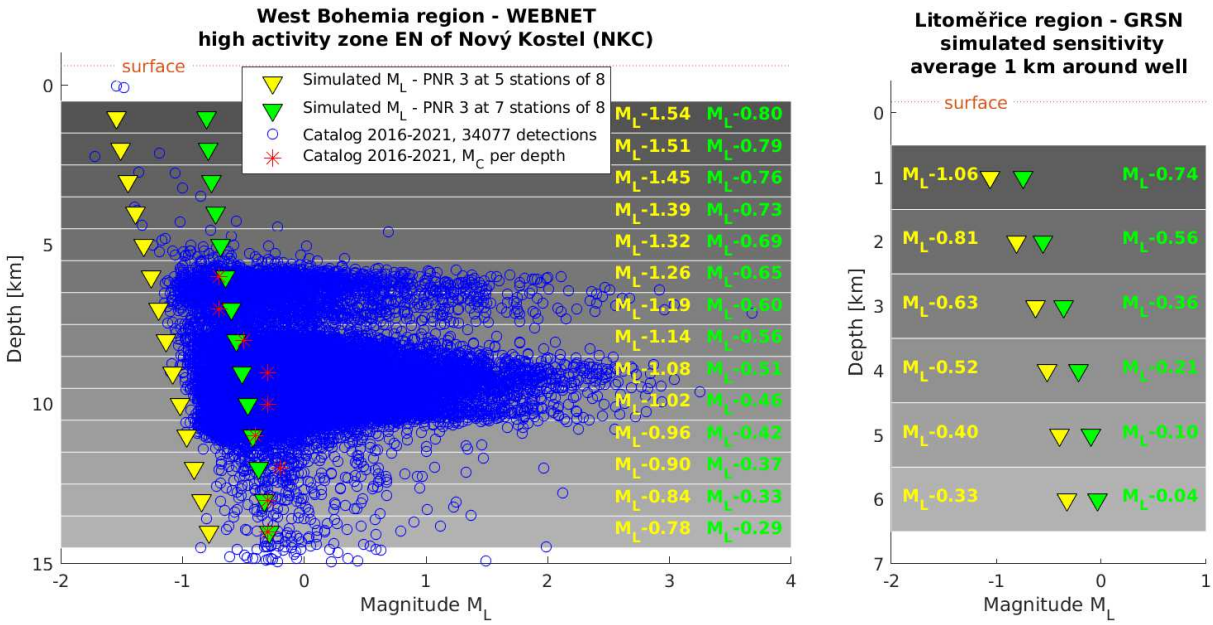

Fig. 11 Results of **simulated sensitivity** per depth in confined regions: minimal detectable M_L in yellow triangles (and yellow M_L values) and M_L of completeness in green triangles (and green M_L values). **WEBNET on the left:** Average network sensitivity simulated in highly active area NE of Nový Kostel (Fig. 6 right), overlaid by seismic activity as detected by automatic detection algorithm in this region (blue circles) and its magnitude of completeness per depth (red star with red label). **GRSN on the right:** Average network sensitivity simulated 2x2km around well.

Doubravová J, Horálek J (2019) Single Layer Recurrent Neural Network for detection of local swarm-like earthquakes—the application. Geophysical Journal International 219(1):672–689. https://doi.org/10.1093/gji/ggz321

Fischer T (2003) Automatic location of swarm earthquakes from local network data. Studia Geophysica et Geodaetica 47:83–98. https://doi.org/10.1023/A:1022251605990

Fischer T, Bachura M (2014) Detection capability of seismic network based on noise analysis and magnitude of completeness. Journal of Seismology 18:137–150. https://doi.org/10.1007/s10950-013-9407-y

Hallo M (2012) Microseismic surface monitoring network design - sensitivity and accuracy. https://doi.org/10.3997/2214-4609.20148336, conference Proceedings, 74^{th} EAGE Conference and Exhibition incorporating EUROPEC 2012, Jun 2012, cp-293-00307

Horálek J, Fischer T, Bouškova A, et al (2000) The western bohemia/vogtland region in the light of the webnet network. Studia Geophysica et Geodaetica 44:107–125. https://doi.org/10.1023/A:1022198406514

Häring MO, Schanz U, Ladner F, et al (2008) Characterisation of the basel 1 enhanced geothermal system. Geothermics 37(5):469–495. https://doi.org/10.1016/j.geothermics.2008.06.002

Institute of Geophysics, Academy of Sciences of the Czech Republic (1991) West bohemia local seismic network. https://doi.org/10.7914/SN/WB, URL https://www.fdsn.org/networks/detail/WB/

Janská E, Eisner L (2012) Ongoing seismicity in the dallas-fort worth area. The Leading Edge 31(12):1462–1468. https://doi.org/10.1190/tle31121462.1

Kværna T, Ringdal F, Schweitzer J, et al (2002) Optimized seismic threshold monitoring – part 1: Regional processing. Pure and applied geophysics 159:969–987. https://doi.org/10.1007/s00024-002-8668-0

Leptokaropoulos K, Gkarlaouni C (2016) A magnitude independent space-time earthquake clustering algorithm (mistic). Bulletin of the Geological Society of Greece 50(3):1359–1368. https://doi.org/10.12681/bgsg.11849

López-Comino J, Cesca S, Kriegerowski M, et al (2017) Monitoring performance using synthetic data for induced microseismicity by hydrofracking at the Wysin site (Poland). Geophysical Journal International 210(1):42–55. https://doi.org/10.1093/gji/ggx148

Mignan A, Werner M, Wiemer S, et al (2011) Bayesian estimation of the spatially varying completeness magnitude of earthquake catalogs. Bulletin of the Seismological Society of America 101:1371. https://doi.org/10.1785/0120100223

Neunhöfer H, Hemmann A (2005) Earthquake swarms in the vogtland/western bohemia region: Spatial distribution and magnitude–frequency distribution as an indication of the genesis of swarms? Journal of Geodynamics 39(4):361–385. https://doi.org/10.1016/j.jog.2005.01.004

Perol T, Gharbi M, Denolle M (2018) Convolutional neural network for earthquake detection and location. Science Advances 4(2):e1700,578. https://doi.org/10.1126/sciadv.1700578

Sereno Jr. TJ, Bratt SR (1989) Seismic detection capability at noress and implications for the detection threshold of a hypothetical network in the soviet union. Journal of Geophysical Research: Solid Earth 94(B8):10,397–10,414. https://doi.org/10.1029/JB094iB08p10397

Shearer PM (2009) Introduction to Seismology, 2nd edn. Cambridge University Press, https://doi.org/10.1017/CBO9780511841552

Trnkoczy A (2012) Understanding and parameter setting of STA/LTA trigger algorithm. Deutsches GeoForschungsZentrum GFZ, Podsdam, https://doi.org/10.2312/GFZ.NMSOP-2_IS_8.1

Wiemer S, Wyss M (2000) Minimum magnitude of completeness in earthquake catalogs: Examples from alaska, the western united states, and japan. Bulletin of the Seismological Society of America 90:859–869. https://doi.org/10.1785/0119990114

Čermáková H, Horálek J (2015) The 2011 west bohemia (central europe) earthquake swarm compared with the previous swarms of 2000 and 2008. Journal of Seismology 19:899–913. https://doi.org/10.1007/s10950-015-9502-3

Šafanda J, Verner K, Franěk J, et al (2020) Geology and geothermal potential in the eastern flank of eger rift (litoměřice area, czech republic). Geothermics 86:101,808. https://doi.org/10.1016/j.geothermics.2020.101808

Supplements

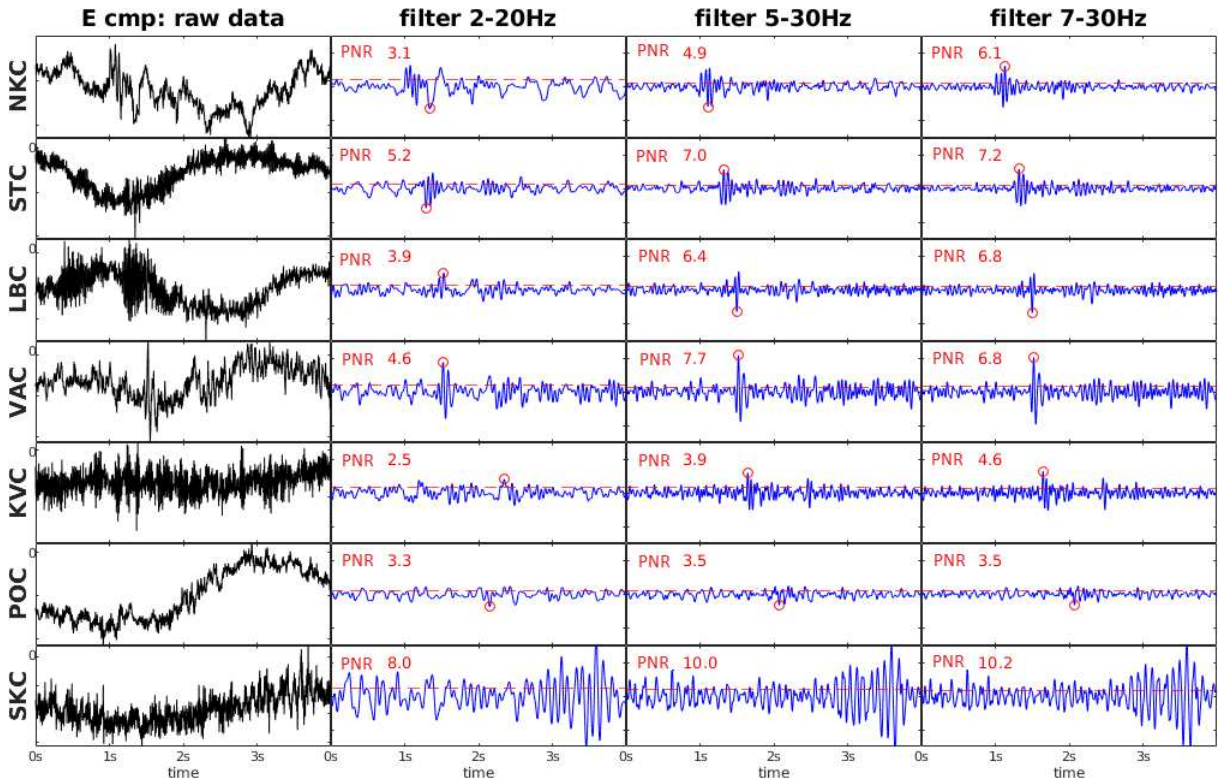

Fig. 1 Filter test. A local seismic event near Nový Kostel, WEBNET: M_L -1.1, depth 5 km, 50.2544 12.4573, 22nd August 2018 13:01:02 UTC: East component of raw data of seven WEBNET stations in black, filtered by band-pass filter 2-20Hz, 5-30Hz and 7-30Hz in blue. Horizontal time axes are similar, vertical amplitude axes are similar only for the blue waveforms. Red dashed line corresponds to the average noise level of the station; the red circle highlights the highest peak labeled with its PNR.

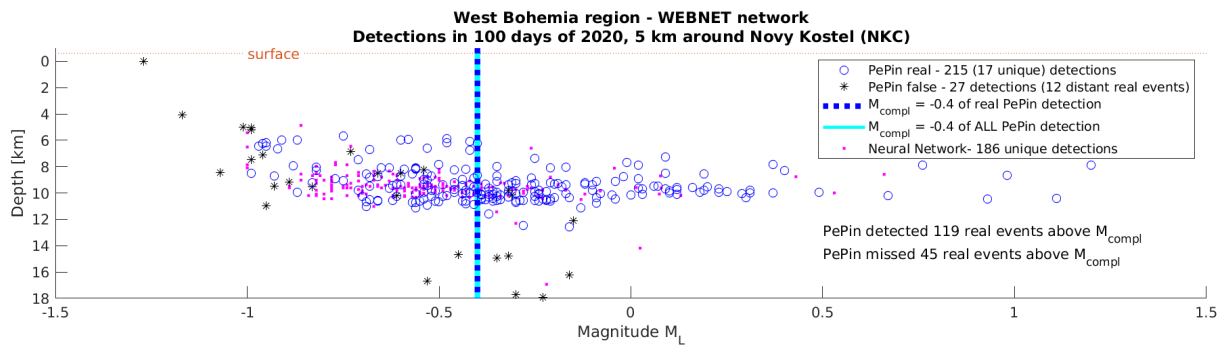

Fig. 2 WEBNET: true + false + missed detections. 242 events detected and located the automatic algorithm (PePin) in a square 10x10 km centered around Nový Kostel. All detections visually checked: 215 recognized as real local events (blue circles), 27 recognized as false detections (black asterisk), including 12 distant events with incorrect location. The magnitude of completeness M_C of PePin detection is not influenced by in/excluding the false detections (Mc by blue and cyan line coincide, derived with a bin size M_L 0.1). Events detected by neural network algorithm and located with manual P and S picks, that were not detected by PePin, are displayed as well (186 magenta dots).

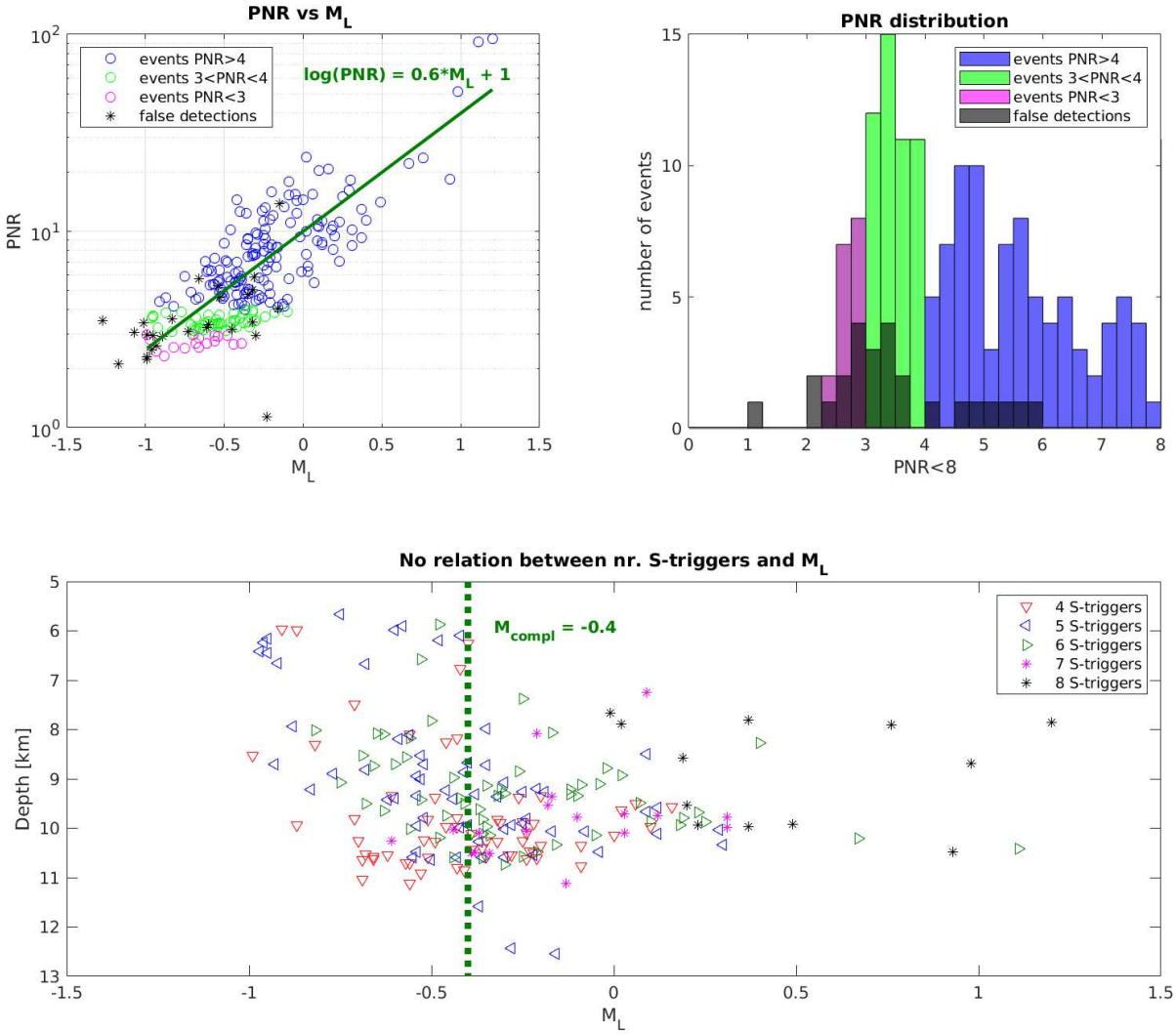

Fig. 3 Minimal **PNR value of PePin detections** in the first 100 days of the year 2020. **Top left:** PNR vs M_L in semi logarithmic scale, real detections fitted by curve log(PNR) = 0.6*M_L + 1 with standard deviation PNR 5.4. **Top right:** a histogram of PNR of real events in colors overlied by a histogram of PNR of false detection in black. **Bottom:** M_L vs depth, color coded by the number of S-wave triggering stations.

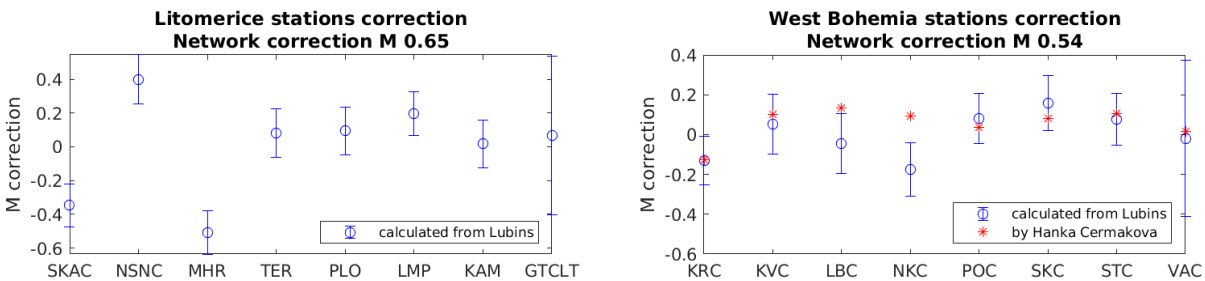

Fig. 4 Station and network corrections of GRSN (left) and WEBNET (right) derived from 48 Lubin events (blue circles with standard deviation as error bars). WEBNET station corrections compared to corrections by Čermáková and Horálek (2015) (red stars).

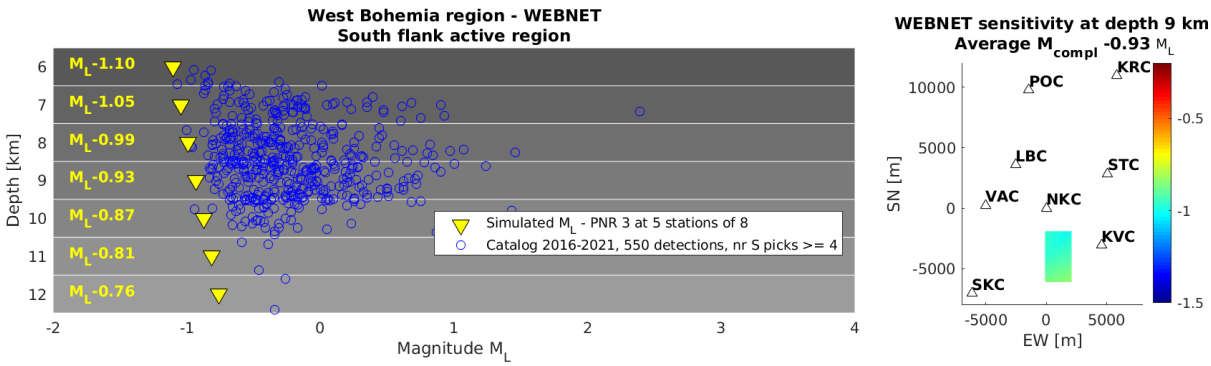

Fig. 5 WEBNET **simulated vs real sensitivity** in south flank active zone. **Left:** Seismic activity as detected by automatic detection algorithm in the South flank of the network. Seismic events displayed as M_L vs depth below mean sea level in blue circles. Average simulated sensitivity in this region (yellow triangles with yellow labels here) is enveloping the observed seismic activity. **Right:** Map view of the south flank region - the simulated sensitivity in depth 9 km (in color).

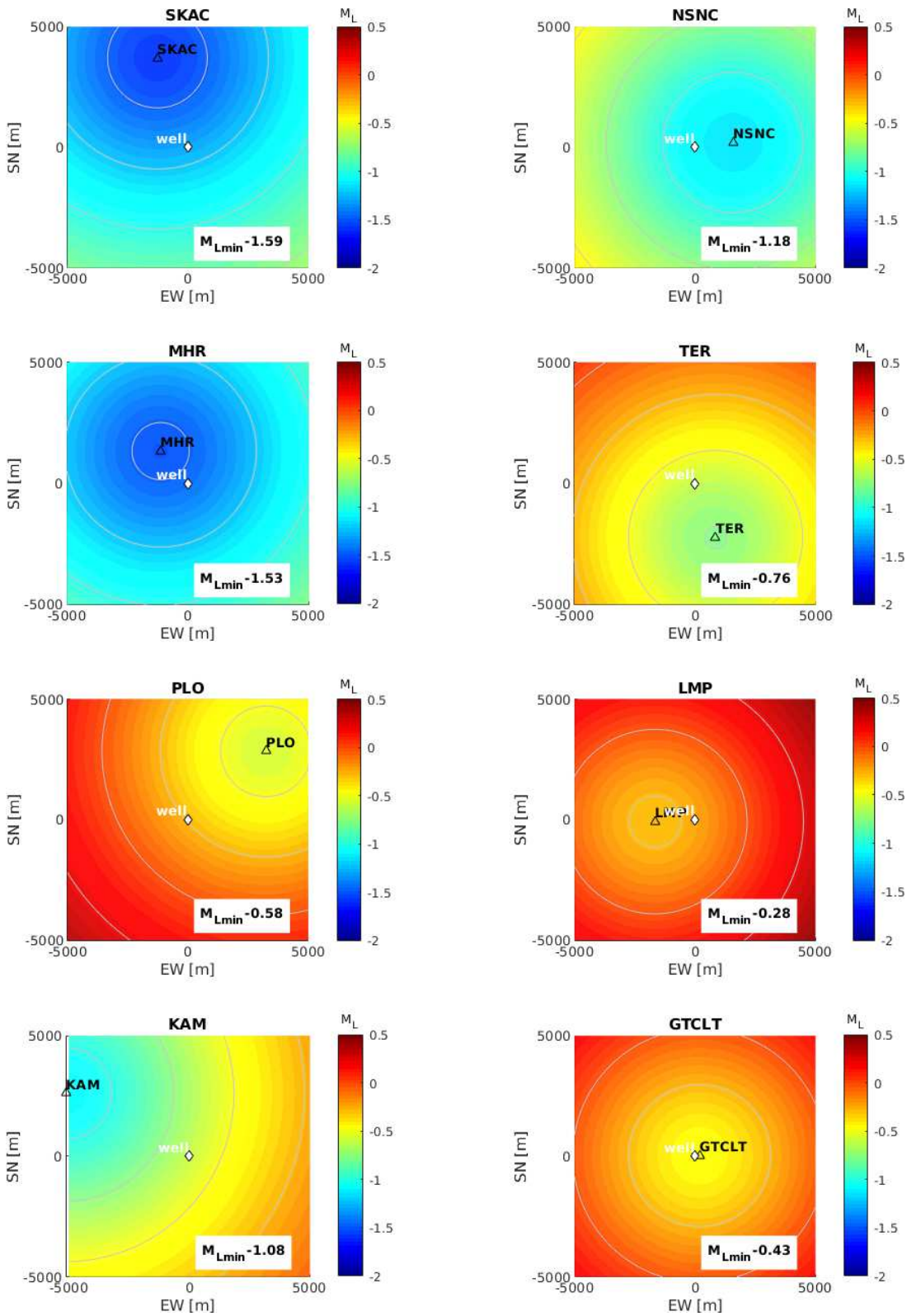

Fig. 6 GRSN: Sensitivity M_L of each single station, at depth 2 km below mean sea level. Grey isolines are spaced by M_L 0.25. Subplot titles note the station name, label represents minimal detectable magnitude at such depth.

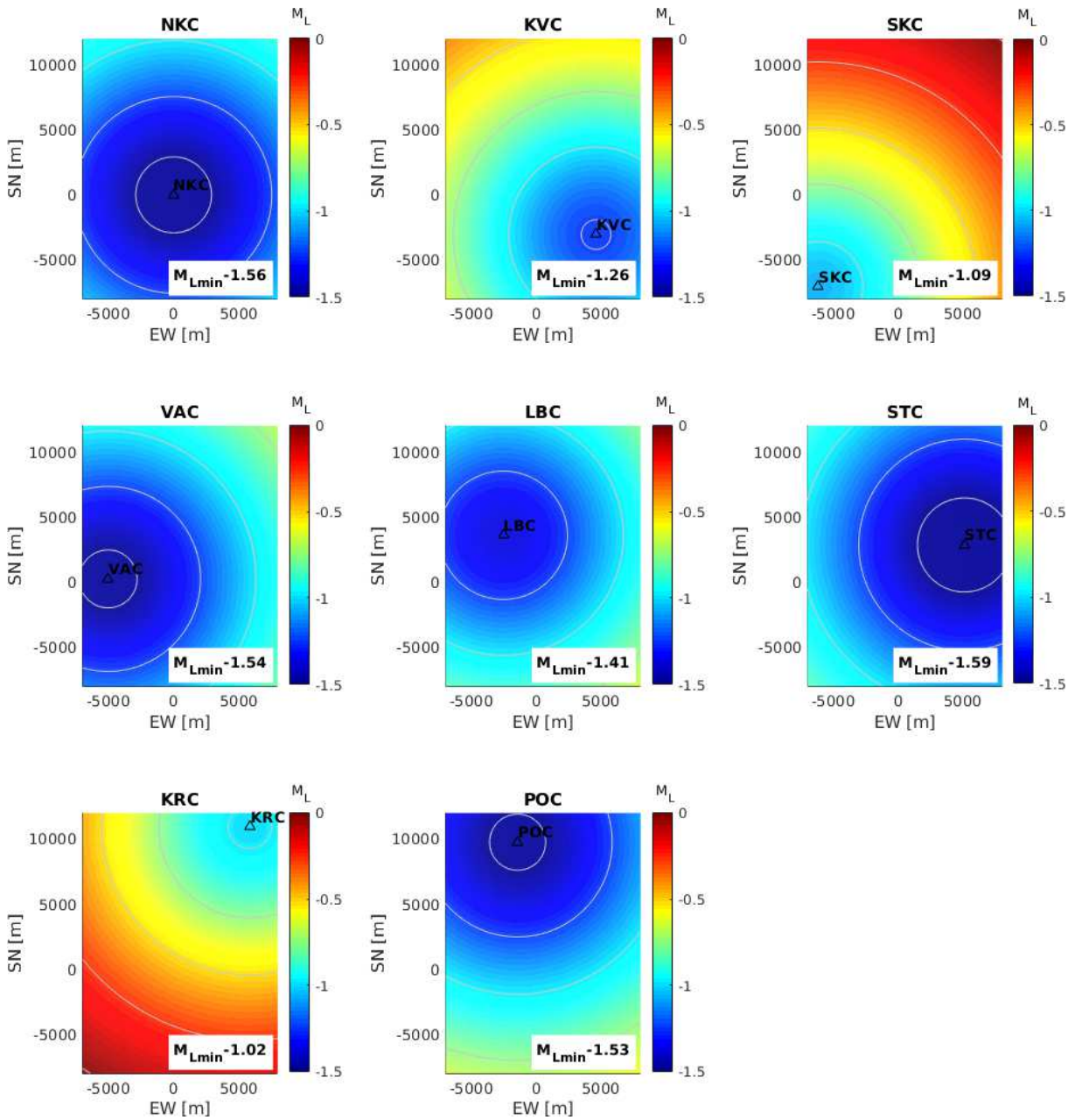

Fig. 7 WEBNET: Sensitivity M_L of each single station, at depth 7 km below mean sea level. Grey isolines are spaced by M_L 0.25. Subplot titles note the station name.